Airy Beam for Free-space Photonic Interconnection: generation strategy and trajectory manipulation

Lei Zhu, Zheng Yang, Songnian Fu, Zizheng Cao, Yuncai Wang, Yuwen Qin, and A. M. J. Koonen

***Abstract*—Self-accelerating beams have attracted worldwide research attentions, due to their intriguingly curved trajectory with localized peak intensity and the characteristic of self-healing after obstacles. We first put forward a generation vector to analytically describe general trajectory manipulation for two dimensional (2D) Airy beam. Based on the successful trajectory manipulation of 2D Airy beam, a 100 Gbps NRZ-OOK real-time free-space photonic interconnection is experimentally demonstrated. Our results indicate that the bending trajectory can break the constraints of traditional free-space photonic interconnection where the receiver has to be set under the condition of line-of-sight. Meanwhile, by taking the power correction factor into account of the beam width variation, we propose a metric of normalized power density (NPD) in order to characterize the power density variation of beam main lobe along the free-space propagation. After calculating the 3 dB NPD range of both Airy beam and Gaussian beam, we identify that the power density of Airy beam main lobe can be maintained for a longer free-space reach than a Gaussian beam with the same minimum width.**

***Index Terms*—Photonic interconnection, Optical beams, Self-accelerating beam, Free-space.**

I. Introduction

Free-space photonic interconnection, offering high bandwidth and flexible parallel connectivity in three-dimensional (3D) space without interference among light paths, is ideally helpful to scale up the performances of indoor [1-2] and outdoor [3] interconnection applications, especially under the chip scenario [4]. Generally, the light path of free-space photonic interconnection is a typical line-of-sight path, directly connecting the transmitter and the receiver. Recently, self-accelerating beams have attracted worldwide research attentions [5-7], due to their intriguingly curved trajectory with localized peak intensity in free-space [8-9] and the characteristic of self-healing after obstacles [10-11]. Such bending trajectory can realize a flexible 3D free-space photonic interconnection. Consequently, the receiver can be flexibly set along the bending trajectory. Meanwhile, the main lobe of self-accelerating beams exhibits the diffraction resistance [12], leading to the free-space reach enhancement without the distinct divergence. Generally, the field of self-accelerating beams can be designed by the caustic theory [9,13], which can be decomposed into a series of Airy functions [9]. Thus, a beam with an Airy shaped envelope is the simplest self-accelerating beam and was first experimentally generated in 2007 [8,14]. As for the transverse field, 1D Airy beam has an Airy shaped variation along only one dimension, while 2D Airy beam can be regarded as two 1D Airy beams multiplexed in the Cartesian coordinate. The trajectory of 2D Airy beam is the vector sum of two trajectory components in two orthogonal directions. Such dynamic manipulation makes 2D Airy beam more suitable than 1D Airy beam for the free-space photonic interconnection. Recently, both image signal transmission by using 2D Airy beam [15] and obstacle evasion optical communication enabled by 1D Airy beam [16] have been reported. However, a comprehensive investigation is compulsory to understand the trajectory manipulation and the free-space propagation characteristics over the bending trajectory.

In this submission, based on a cubic-type phase mask, we first put forward a generation vector to analytically describe the general parabolic trajectory manipulation for 2D Airy beam. Then real-time 100 Gbps free-space photonic interconnection is demonstrated to verify the trajectory manipulation and compare the interconnection performance among 1D Airy beam, 2D Airy beam, and traditional Gaussian beam. Since the experimentally generated self-accelerating beams are the truncated version [14], it cannot always maintain its trajectory along the free-space propagation. Thus, the width of beam main lobe for the self-accelerating beam has been previously used to evaluate the propagation characteristic, then a diffraction-free phenomenon has been identified for the self-accelerating beams, based on the fact that the width of self-accelerating beam main lobe grows much slower than Gaussian beam does [9]. However, we identify that the power density distribution of beam is suitable for evaluating the free-space range of photonic interconnection. Hence, we introduce a normalized power density (NPD) of beam main lobe to evaluate the range of free-space photonic interconnection where the bending trajectory can be maintained, for the ease of beam selection.

Manuscript received Apr, 2020. This work was partially supported by National Key R&D Program of China (2018YFB1801301), the National Natural Science Foundation of China (61875061), the Program for Guangdong Introducing Innovative and Entrepreneurial Teams, NOW Zwaartekracht programme on Integrated Nanophotonic, the Netherlands, and ERC Advanced Grant BROWSE project, EU. (*Corresponding authors: Songnian Fu*).

Lei Zhu, Zheng Yang, are with Wuhan National Laboratory for Optoelectronics, and School of Optical and Electronic Information, Huazhong University of Science and Technology (HUST), Wuhan 430074, China (email: zhulei@hust.edu.cn; yangzheng@hust.edu.cn;).

Songnian Fu, Yuncai Wang, and Yuwen Qin are with School of Information Engineering, Guangdong University of Technology, and also with Guangdong Provincial Key Laboratory of Photonics Information Technology, Guangzhou, 510006, China (email: songnian@gdut.edu.cn, wangyc@gdut.edu.cn, qinyw@gdut.edu.cn).

Zizheng Cao and A. M. J. Koonen are with the Institute for Photonic Integration, Department of Electrical Engineering, Eindhoven University of Technology, the Netherlands (email: z.cao@tue.nl; a.m.j.koonen@tue.nl).

II. GENERATION VECTOR OF AIRY BEAM

The self-accelerating beams can be designed with arbitrary trajectories according to the caustic theory, from the either Fourier or real space modulation. The generated beam occurs at the far-field for the Fourier modulation, leading to a high quality in comparison with the beam generated by real space modulation, when the pixel discretization and phase modulation error of spatial light modulator (SLM) are taken into account. Hence, the investigation of Airy beam generation in current submission is based on the Fourier modulation with the help of a lens. In order to generate Airy beam, a Gaussian beam is modulated by a phase type SLM with cubic-type phase mask. Then, after the inverse Fourier transformation (IFT) by a lens, the Airy beam can be obtained. The optical envelope of a Gaussian beam after the spatial phase modulation is $E = E_g T_{SLM}$, where $E_g = \exp\left(-a_x k_x^{\,2} - a_y k_y^{\,2}\right)$ is the envelope of input Gaussian beam at the SLM plane, $k_x = 2\pi x_{SLM} x_0 / (\lambda f)$ is the normalized wave number, x_0 is the transverse scale in the X direction, f is the focal length of lens, x_{SLM} is the transverse coordinate at the SLM plane, λ is the operating wavelength, $a_x = \left[f/(k x_0 \omega)\right]^2$ and $a_y = \left[f/(k y_0 \omega)\right]^2$ are decay factors of experimentally generated Airy beam and determined by the waist radius of the input Gaussian beam together with the transverse scale, $k = 2\pi/\lambda$ is the wave number, and T_{SLM} is the cubic type phase mask to be loaded into the SLM, as shown in Eq.(1)

$$\begin{aligned} T_{SLM} &= \exp\left[i\left(1/3 k_x^{\,3} + n_x k_x^{\,2} + l_x k_x\right)\right] \\ &\times \exp\left[i\left(1/3 k_y^{\,3} + n_y k_y^{\,2} + l_y k_y\right)\right] \end{aligned} \tag{1}$$

where n_x , l_x , n_y and l_y are dimensionless variables. We define a generation vector $\vec{Ph} = \left[x_0, n_x, l_x, y_0, n_y, l_y \right]$ to describe the choice of the phase mask, where the first three items are responsible for the X component of 2D Airy beam, the other three items account for the Y component of the 2D Airy beam, x_0 and y_0 are the transverse scales of 2D Airy beam in the X and Y directions, respectively. From Eq. (1), after angular spectrum propagation and IFT, we can derive the transverse envelope of the 2D Airy beam along the propagation distance as $\varphi(x, y, z) = A(x, z) B(y, z)$,

$$\begin{aligned} A(x,z) &= Airy\left[\frac{x}{x_0} - \frac{1}{4}\left(\frac{z}{k x_0^{\,2}} + 2n_x \right)^2 + l_x + a_x^{\,2} - i a_x \left(\frac{z}{k x_0^{\,2}} + 2n_x \right) \right] \\ &\exp\left[a_x \left(\frac{x}{x_0} + l_x + a_x^{\,2} \right) - \frac{1}{2} a_x \left(\frac{z}{k x_0^{\,2}} + 2n_x \right)^2 - \frac{1}{3} a_x^{\,2} \right] \\ &\exp\left\{ i\left[\frac{1}{12}\left(\frac{z}{k x_0^{\,2}} + 2n_x \right)^3 - \frac{1}{2}\left(\frac{x}{x_0} + l_x + 2a_x^{\,2} \right)\left(\frac{z}{k x_0^{\,2}} + 2n_x \right) \right] \right\} \end{aligned} \tag{2}$$

where $B(y, z)$ has the same expression but with the last three parameters of the generation vector. By setting the real part of the Airy function equal to zero [9], we can obtain the trajectory

$$\begin{cases} x = x_0 \left[\frac{1}{4}\left(\frac{z}{k x_0^{\,2}} + 2n_x \right)^2 - l_x - a_x^{\,2} \right] \\ y = y_0 \left[\frac{1}{4}\left(\frac{z}{k y_0^{\,2}} + 2n_y \right)^2 - l_y - a_y^{\,2} \right] \end{cases} \tag{3}$$

It is interesting to identify that, the trajectory of 2D Airy beam can be composed into two orthogonal parabolic curves along X and Y directions. By taking X direction as an example, n_x and l_x determine the apex position of parabola as $x = -x_0\left(l_x + a_x^{\,2}\right)$ and $z = -2n_x k x_0^{\,2}$. Please note that the quadric, linear, and constant terms in Eq. (3) can be independently manipulated by choosing the suitable generation vector $\vec{Ph}$, enabling the flexible trajectory design. In particular, when both $n_x^{\,2} = l_x$ and $n_y^{\,2} = l_y$ are simultaneously satisfied, Eq. (3) can be simplified to the same equations as shown in previous literature [17-18]. Thus, Eq. (3) is the general results of 2D Airy beam for the purpose of flexible trajectory manipulation.

III. TRAJECTORY VERIFICATION AND FREE-SPACE PHOTONIC INTERCONNECTION EXPERIMENTS

The main lobe of the self-accelerating beams travels along the bending trajectory, which possesses the most energy of beam. As a result, a free-space photonic interconnection can be realized by its power-localized bending trajectory. In this section, we first carry out an experiment to verify the 2D Airy beam trajectory manipulation, then demonstrate a proof-of-concept 100Gb/s real-time free-space photonic interconnection.

A. Experimental setup

The real-time free-space photonic interconnection system is schematically shown in Fig. 1. At the transmitter side, we utilize four transmitters with a channel spacing of 0.8 nm at the C-band. The aggregated data rate after the wavelength division multiplexing (WDM) is 4×25 Gb/s. To generate a 25 Gbps NRZ-OOK signal, each transmitter consists of a distributed feedback (DFB) laser with a linewidth less than 10 MHz, a polarization controller (PC), and a Mach-Zehnder modulator (MZM, Photline MX-LN-40) with a 3 dB modulation bandwidth of 30 GHz. The operating wavelengths of four transmitters are 1548.54 nm, 1549.34 nm, 1550.14 nm, and 1550.94 nm, respectively. We use a four-channel bit error ratio (BER) tester (BERTWave E425B) for the ease of real-time characterization. After being amplified by four electrical amplifiers (EA), the electronic signals drive the MZMs. Inset (a) of Fig. 1 shows the corresponding optical spectrum. Before the optical signal is launched into the free-space channel, we utilize an erbium-doped fiber amplifier (EDFA1) to manage the optical power. At the receiver side, we use another optical

This article has been accepted for publication in a future issue of this journal, but has not been fully edited. Content may change prior to final publication. Citation information: DOI 10.1109/JLT.2020.3014893, Journal of Lightwave Technology

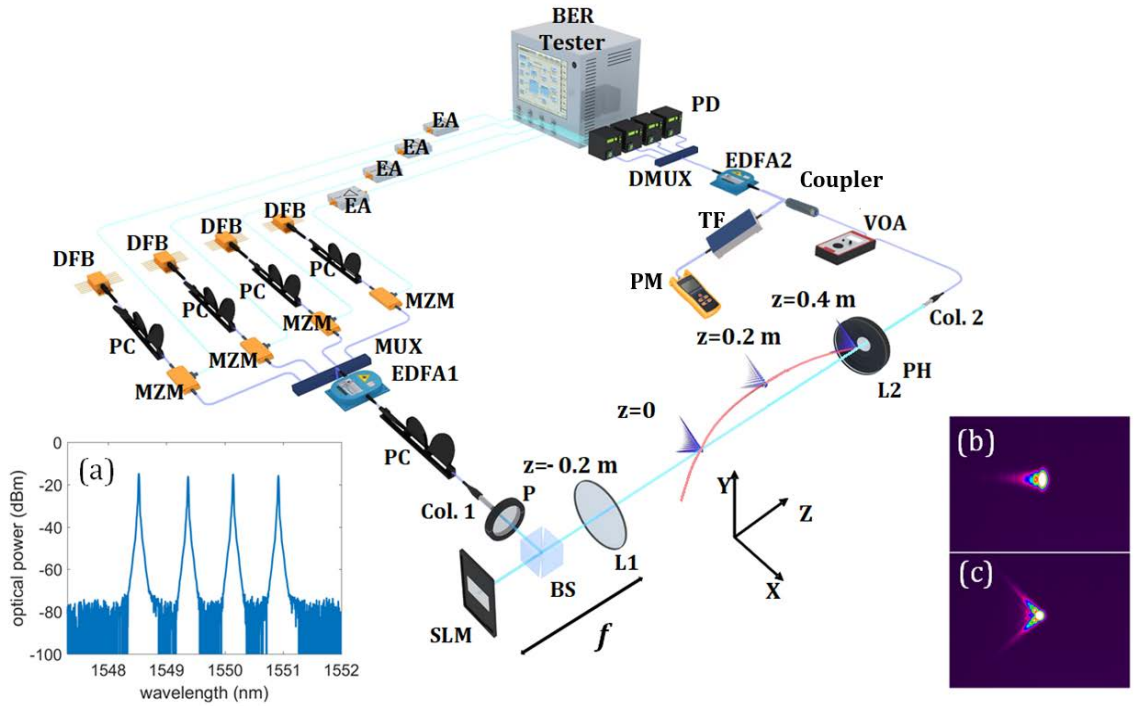

Fig. 1. Schematic of free-space photonic interconnection. Col., collimator; P, polarizer; BS, beam splitter; SLM, spatial light modulator; PH, pinhole; VOA, variable optical attenuator; TF, tunable filter; PM, power meter. Inset (a): optical spectrum of 4×25 Gbps NRZ-OOK signal. Inset (b): intensity profile of 1D Airy beam. Inset (c): intensity profile of 2D Airy beam.

amplifier (EDFA2) to amplify the received optical signal. After wavelength division de-multiplexing and optical-to-electrical conversion by four photodetectors (PD, U2T MPRV1332A) with 3 dB bandwidth of 31 GHz, the signals are collected for error-counting over more than 30 seconds to avoid the stochastic fluctuation. A variable optical attenuator (VOA) is set before EDFA2 to adjust the received optical power. Meanwhile, a 90:10 optical coupler together with a tunable filter (TF) and a power meter (PM) are used to monitor the received optical power, for the ease of performing BER testing. The light at standard single mode fiber (SSMF) output is collimated to a Gaussian beam with a waist radius of about 1.75 mm. After passing through a polarizer (P) and a beam splitter (BS), the light is modulated by an SLM (PLUTO-TEL-013, HOLOEYE) with resolutions of 1920x1080 and a pixel pitch of 8 μm. After the IFT with the help of lens L1, 2D Airy beam is finally generated. The focal lengths of L1 and L2 are both 0.2 m, and the initial point z=0 is set at the back focal plane of L1 for the ease of defining the free-space propagation of the generated Airy beam. As for the receiver side, L2 is placed at z=0.4 m to couple the light into the SSMF. A pinhole (PH) with a radius of 1.75 mm is placed right after L2, for the purpose of reducing the receiver aperture.

B. Verification of trajectory manipulation

To verify the capability of trajectory manipulation, we experimentally generate various 2D Airy beams. The experimental setup of 2D Airy beam generation is shown in Fig. 1 without the receiver part. An infrared CCD camera (SP620U-1550, Ophir) captures the intensity profiles of 2D Airy beam at variable free-space propagation distances from the back focal plane of L1. The CCD camera is mounted on a rail, allowing it to move along the Z direction. Fig. 2 shows the experimentally captured trajectories of four different 2D Airy beams, together with their calculated trajectories. The theoretical predictions (solid curves) are in good agreement with the experimental observations (dashed curves).

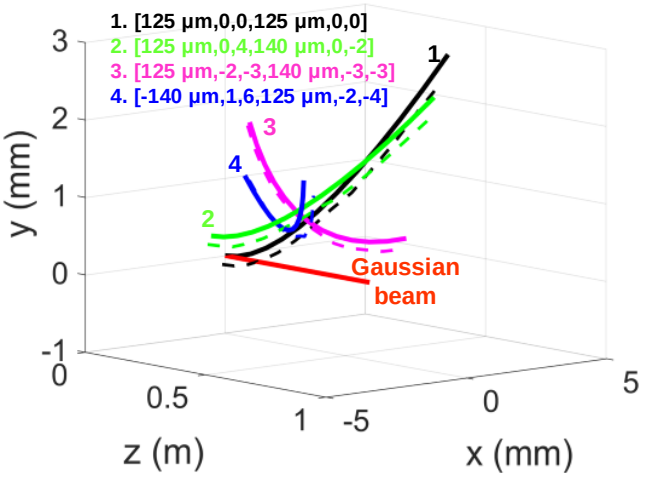

Fig. 2. Experimental results of 2D Airy beam trajectory manipulation.

C. Photonic interconnection results

We take two-step experimental verifications for the proposed free-space photonic interconnection system. The first step is to compare the interconnection performance among three beams, including 2D Airy beam, 1D Airy beam, and Gaussian beam, without the obstacle setting. Next, we try to evaluate the capability of obstacle evasion among three beams. When an obstacle is set at a specific point of the line-of-sight light path, we can design a 2D Airy beam with the curved trajectory

according to Eq. (3), in order to avoid the obstacle. In our experiments, the obstacle is set at z=0.2 m. Since the apex point of parabolic trajectory is the highest position of trajectory, we intentionally set the obstacle at the apex position, in order to enhance the capability of obstacle evasion. The apex height of the parabolic trajectory can be optimized according to the height of obstacle. When a higher obstacle is set, we can select an appropriate trajectory with a higher apex to avoid the obstacle. In order to simply make a performance comparison, the parameters of three beams are fixed and an obstacle with variable height is utilized in the experiment. The generation vector of 2D Airy beam is $[115\ \mu m, -1.87, 3.48, 115\ \mu m, -1.87, 3.48]$ and that of 1D Airy beam is $[115\ mm, -1.87, 3.48, 0, 0, 0]$. Thus, 1D Airy beam is set as a subset of 2D Airy beam. The decay factor for both 1D Airy beam and 2D Airy beam is 0.6. As a result, the trajectories of both 1D Airy beam and 2D Airy beam can pass through the PH and then be coupled into the SSMF. Both parabolic trajectories have their apex at z=0.2m, where the obstacle is set. Meanwhile, the Gaussian beam has an experiment waist of 1.75 mm.

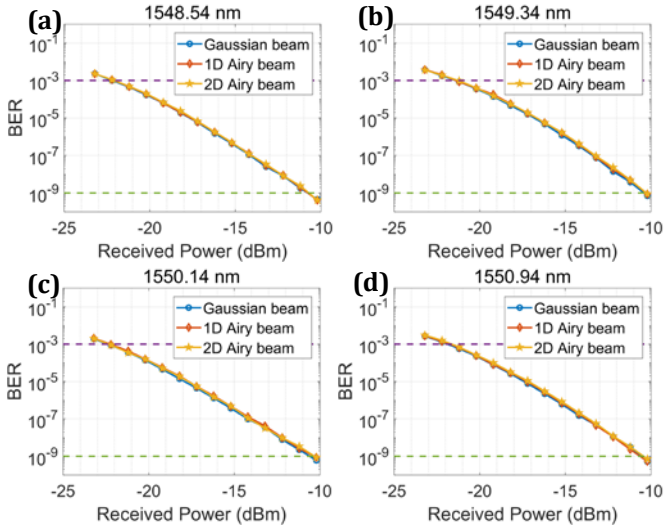

Fig. 3. Real-time BER performances of 4×25 Gbps free-space photonic interconnection

As shown in Fig. 3, real-time BER performances among three beams without the obstacle setting are characterized first with respect to the received power of each wavelength channel. The receiver sensitivity of three optical beams at the specific wavelength is almost identical. However, the fluctuations of receiver sensitivity among four wavelengths are 0.45 dB and 1.2 dB, respectively, when two BER thresholds of 1e-9 and 1e-3 are set. Generally, the BER characterization without the use of forward error correction code must reach the BER threshold of 1e-9, in order to satisfy the objective of real-time photonic interconnection. Due to the fluctuation of modulation depth and drift of optimal bias among four independent transmitters, it is challenging to maintain the quality of optical signal the same for four wavelength channels. Since the performance difference among three beams at the single specific wavelength is trivial, we conclude that the BER performance is mainly determined by the received power of each optical channel, instead of the beam selection. Our experimental results verify that the self-accelerating beams can be utilized for free-space photonic interconnection, when the main lobe can be received.

Next, we insert an opaque thin rectangular plate at the light path to investigate the performance improvement assisted by the bending trajectory of Airy beam. The plate is set at z=0.2 m, with one top edge parallel to the Y-axis, and the plate can be transversely moved along the X-axis. The distance between the top edge and the Z-axis is denoted as h. The phase mask for generating 2D Airy beam is rotated 45 degrees to obtain a parabolic trajectory in the X-O-Z plane, so that the main lobe can travel away from the Z-axis along the X direction with a longer distance. At first, without the plate, the received optical power of each wavelength is set to -10 dBm for all three optical beams by managing the amplifying ability of EDFA1 at the transmitter side. Then, with the moving plate at the path of each beam, the BER performance is measured, as shown in Fig. 4. Initially, the BER curves overlap with each other, because none of three beams is blocked by the plate. When the distance h increases, Gaussian beam starts to be partially blocked first.

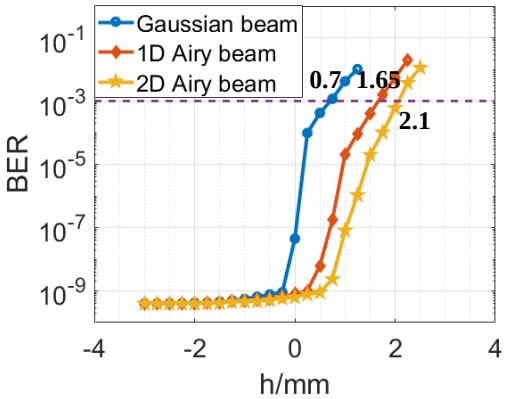

Fig. 4. Real-time BER performances comparison with moving opaque plate.

Due to the bending trajectory and self-healing of the main lobe, the BER performances of 2D and 1D Airy beam are better than that of Gaussian beam. Moreover, since the trajectory of 2D Airy beam is the vector sum of two 1D Airy beams, the trajectory of 2D Airy beam can travel away from the Z-axis with a longer transverse distance. If we assume that the photonic interconnection interrupts when BER is higher than 1e-3, we can identify that the tolerance of h for three beams are 0.67 mm, 1.65 mm and 2.1 mm, respectively.

IV. Discussions of Beam Selection

The bending trajectory of self-accelerating beams reveals the movement of beam main lobe in free-space. Therefore, the photonic interconnection can keep the function by setting the receiver along the bending curve. However, the bending trajectory cannot always be maintained the same as the theoretical design. Due to the limited aperture or limited spatial bandwidth of the experimentally generated beams, such bending trajectory is a transient state process. For 2D Airy beam, it is generated by the Fourier modulation, and the boundary between the main lobe and the side lobes will finally

disappear and merge into a Gauss-shaped beam, with the growing free-space propagation distance [19]. Consequently, a metric is indispensable to evaluate the free-space propagation characteristic of the self-accelerating beam and identify the range of bending trajectory, in order to provide a guidance to optimize the free-space interconnection reach. In our next discussion, only X direction is considered for the ease of discussion.

In order to evaluate the free-space propagation characteristic of optical beams, the beam size is often used to derive the Rayleigh range according to the size variation. Whereas, due to the power exchange between the main lobe and side lobes for the self-accelerating beams during the free-space propagation, only the variation of beam width is not sufficient to evaluate the free-space propagation characteristics for the self-accelerating beams. Therefore, we put forward a power correction factor $\frac{P_m(z)}{P_{m0}}$ to describe the beam width variation, and a metric of NPD is defined for the main lobe of the self-accelerating beams

$$NPD = \frac{width_0}{width(z)} \frac{P_m(z)}{P_{m0}} \tag{4}$$

where $width(z)$ denotes the width of main lobe along the free-space propagation, and $width_0$ is the minimum value of $width(z)$, $P_m(z)$ represents the power possessed by the main lobe of the self-accelerating beams, and P_{m0} is the maximum value of $P_m(z)$. The NPD can characterize the variation of power density for the main lobe during the free-space propagation, which is essential for the free-space photonic interconnection, because the BER performance is sensitive to the spatial power density when the receiver aperture is finite in practice. As a result, we can set an NPD threshold to define the range of transient state where the self-accelerating beams can maintain its bending trajectory. Similar to the concept of 3 dB bandwidth, we set the threshold of 0.5 for the below discussion. The 3 dB NPD range is similar to the Rayleigh range for Gaussian beam, because the power correction factor is $\frac{P_m(z)}{P_{m0}}=1$, even though the width of Gaussian beam varies quickly along the free-space propagation. For the ease of understanding, we start to explain the definition of variables first. The width of main lobe $width(z)$ is calculated as the full-width-half-max (FWHM) of main lobe intensity distribution. Meanwhile, we calculate $P_m(z)$ as the power within the FWHM to represent the power possessed by the main lobe. According to the Eq. (2) and (3), we can find that the profile of Airy beam is only determined by the transverse scale x_0 and decay factor a_x. The parameter n_x moves the Airy beam longitudinally and l_x shifts the beam transversely. As a result, n_x and l_x determine the apex of the parabolic curve. In order to obtain independent results on the scale of the beam, the transversal scale and longitudinal scale can be normalized to

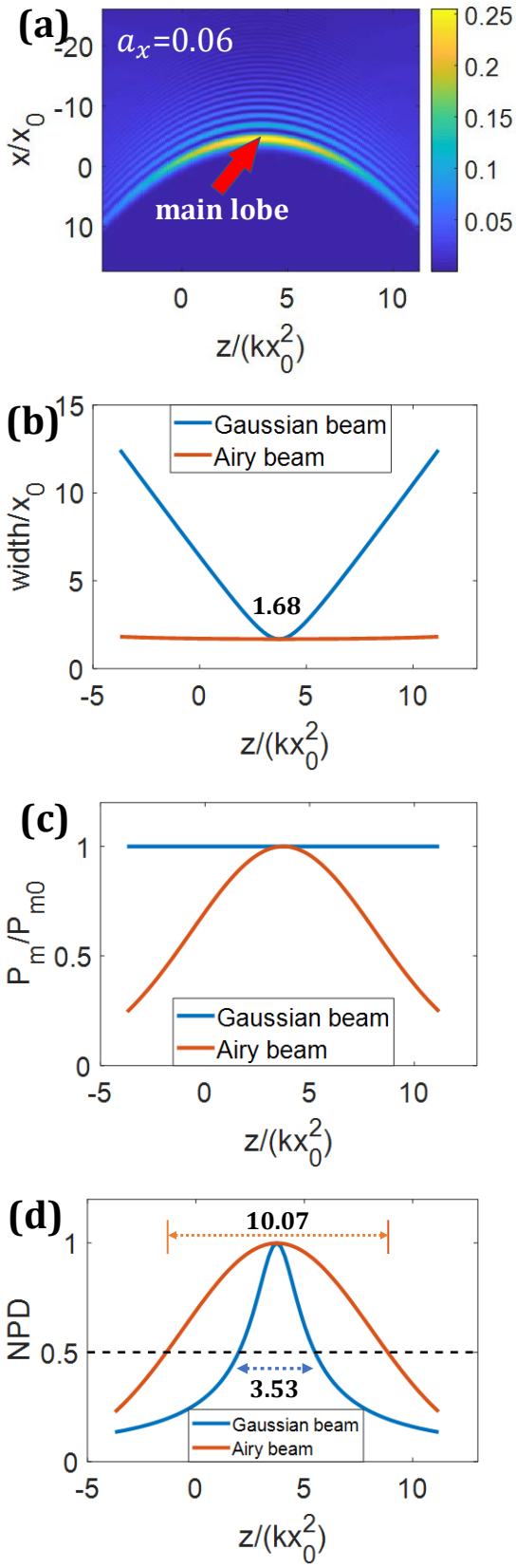

Fig. 5. Comparison between Gaussian beam and an Airy beam with the same minimum width. (a) the intensity profile of the Airy beam; (b) the width comparison; (c) the power variation with growing propagation distance. (d) comparisons of the NPD and the 3 dB NPD range.

dimensionless variables as x / x_0 and $\frac{z}{kx_0^2}$, respectively.

A. Propagation comparisons between Gaussian and Airy beams

The intensity profile of 2D Airy beam is schematically shown in Fig. 5(a), based on the generation vector of $[x_0, -1.87, 3.48, y_0, -1.87, 3.48]$ together with a decay factor of $a_x = a_y = 0.06$. The main lobe of 2D Airy beam propagates over a parabolic curve predicted by Eq. (3), with its apex at the position $\frac{z}{kx_0^2} = -2n_x = 3.74$. On the contrary, since the Gaussian beam only has one beamlet, the main lobe of Gaussian beam is the entire beam itself, which travels over a line. As shown in Fig. 5(b), the main lobe width of Airy beam is nearly unchanged during the free-space propagation interval from $z = -4kx_0^2$ to $z = 11kx_0^2$, and it reaches the minimum value of $width_0 = 1.68x_0$ at the apex of the parabolic trajectory. A Gaussian beam with the same minimum FWHM of $width_0 = 1.68x_0$ is also calculated, and the results are shown together with Airy beam in Fig. 5(b). We can find that, with the identical minimum width, the Gaussian beam spreads quickly with the growing free-space propagation distance. However, the main lobe of Airy beam can propagate under an anti-diffraction manner with a curved trajectory. The power possessed by the main lobe for both Airy beam and Gaussian beam along the free-space propagation is calculated in Fig. 5(c). The Gaussian beam always has a Gaussian-shaped intensity profile during the free-space propagation, though its beam width experiences a rapid expansion. Hence, the power of main lobe keeps constant during the free-space propagation. On the contrary, the power of the main lobe for the Airy beam suffers a reduction with the free-space propagation on both sides of the apex position. By taking those two factors including both beam width and power of main lobe into account, we can obtain the NPD of Airy beam and Gaussian beam, as shown in Fig. 5(d). Both Airy beam and Gaussian beam have a deduction of NPD, due to the diffraction effect arising in the free-space propagation. The dominate factor to affect the NPD of Gaussian beam is the dramatically increasing beam width. However, as for the Airy beam, the major factor is the varied power of the main lobe. The lengths of corresponding 3 dB NPD range L_{3dB} for Airy beam and Gaussian beam are $10.07kx_0^2$ and $3.53kx_0^2$, respectively. It is interesting to identify that both 3 dB NPD ranges of two optical beams vary quadratically with the transversal scale x_0. In addition, the Airy beam possesses a much longer L_{3dB} than that of Gaussian beam, indicating that the main lobe of Airy beam can propagate in a diffraction resistant way. Hence, Airy beam is beneficial for the long reach of free-space photonic interconnection. Therefore, the metric of NPD is valid to evaluate the free-space propagation of the self-accelerating beam and Gaussian beam. Moreover, we can obtain the 3 dB NPD range where the

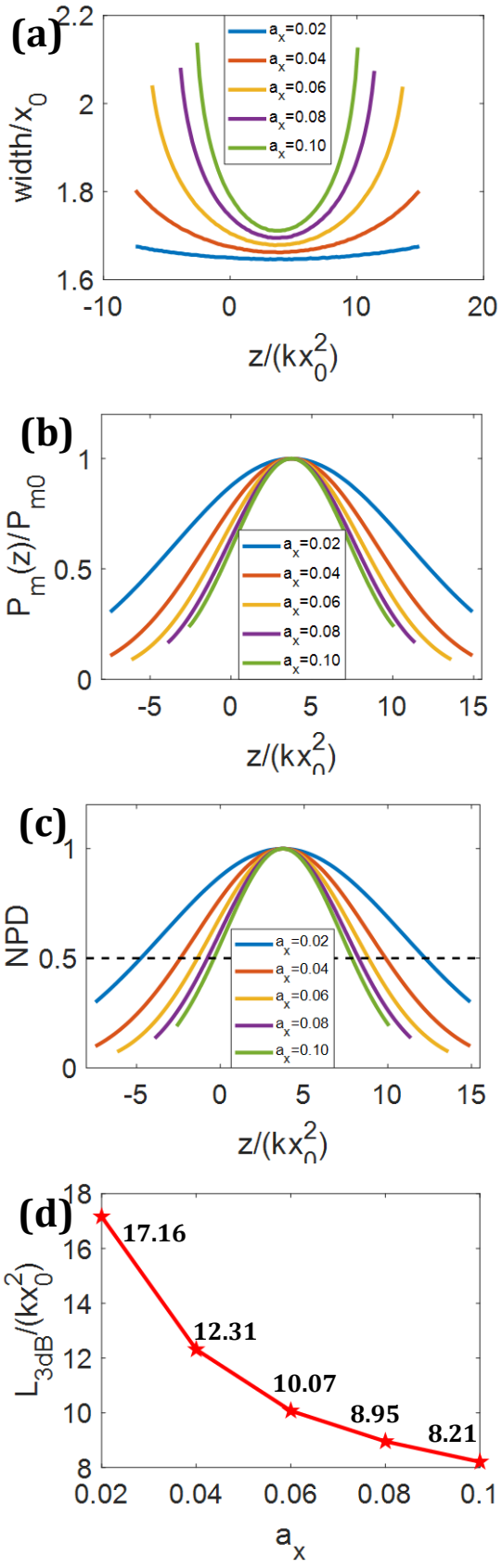

Fig. 6. Effect of decay factor on the Airy beam free-space propagation. (a) the width, (b) the power variation of main lobe, (c) NPD, (d) 3 dB NPD range of five Airy beams with decay factors of 0.02, 0.04, 0.06, 0.08, 0.10.

trajectory of self-accelerating beams can be maintained. Despite of the bending trajectory, the power density of main lobe for Airy beam can be maintained for a longer reach than that of Gaussian beam.

B. Effect of decay factor

For the Fourier modulation method to generate Airy beam, the decay factor a_x has an influence on the free-space propagation performance. In this section, five Airy beams with the same generation vectors $[x_0, -1.87, 3.48, y_0, -1.87, 3.48]$ but different decay factors from 0.02 to 0.1 are numerically compared. According to the Eq. (3), the effect of decay factor on the trajectory can be neglected, due to its minor value. As a result, five Airy beams have almost the same trajectory with the same apex point at $z = 3.74kx_0^2$.

We calculate the FWHM width and the power of main lobe, as shown in Fig. 6 (a) and (b), respectively. The width of main lobe presents a U-shape curve, and it reaches the minimum value at the apex point of the parabolic trajectory. With the increase of the decay factor, the minimum width enlarges, and the width expansion rate increases on the both sides of the minimum value. On the other hand, the power possessed by main lobe reduces faster with larger decay factor. Then the NPD is calculated in Fig. 6(c) and the corresponding length of 3 dB NPD range L_{3dB} is shown in Fig. 6(d). We find that the NPD comes to its peak at the apex point of the trajectory, and the length of 3 dB NPD range declines with the increase of the decay factor. The reduction of NPD on both side of the apex point, can be attributed to the limited spatial bandwidth of the generated Airy beam. For the designated parabolic trajectory, the slope of the trajectory increases as the beam propagates away from the apex point. Consequently, the spatial bandwidth of optical beam has to be enlarged if a longer 3dB NPD range is desired. Overall, the 3 dB NPD range of typical Airy beam can be optimized by the decay factor.

V. CONCLUSION

We put forward a generation vector to analytically describe a general trajectory manipulation for 2D Airy beam. Based on the successful trajectory manipulation of Airy beam, a 100 Gbps NRZ-OOK real-time free-space photonic interconnection is experimentally demonstrated. Our results indicate that the receiver can be set under the condition of non-line-of-sight along the curved trajectory. Meanwhile, 2D Airy beam has more powerful obstacle-evasion ability than that of 1D Airy beam. Since the trajectory of self-accelerating beam is a transient state process, a metric of NPD is proposed to evaluate such process. We identify that the power density of Airy beam main lobe can be maintained for a longer distance than that of Gaussian beam. What's more, the range of free-space reach can be optimized with respect to the decay factor. In addition to the trajectory manipulation, we believe that such metric is helpful for the design of free-space photonic interconnection enabled by the self-accelerating beams. It could be utilized in other power sensitive applications of self-accelerating beams, such as optical tweezer and micro-machining.

REFERENCES

[1] T. Koonen, "Indoor Optical Wireless Systems: Technology, Trends, and Applications," *J. Lightw. Technol.*, vol. 36, no. 8, pp. 1459-1467, 2018.

[2] H. Haas, L. Yin, Y. Wang and C. Chen, "What is LiFi?", *J. Lightw. Technol.*, vol. 34, no. 6, pp. 1533-1544, Mar. 2016.

[3] M. P. J. Lavery, C. Peuntinger, K. Günthner, P. Banzer, D. Elser, R. W. Boyd, M. J. Padgett, C. Marquardt and G. Leuchs, "Free-space propagation of high-dimensional structured optical fields in an urban environment," *Sci. Adv.*, vol. 3, no. 10, pp. e1700552, Oct. 2017.

[4] C. García-Meca, S. Lechago, A. Brimont, A. Griol, S. Mas, L. Sánchez, L. Bellieres, N. S. Losilla and J. Martí, "On-chip wireless silicon photonics: from reconfigurable interconnects to lab-on-chip devices," *Light: Science & Applications*, vol. 6, no. 9, pp. e17053, Mar. 2017.

[5] J. Baumgartl, K. Dholakia and M. Mazilu, "Optically mediated particle clearing using Airy wavepackets," *Nat. Photonics*, vol. 2 no. 11, pp. 675-678, Nov. 2008.

[6] A. Mathis, F. Courvoisier, L. Froehly, L. Furfaro, M. Jacquot, P. A. Lacourt and J. M. Dudley, "Micromachining along a curve: Femtosecond laser micromachining of curved profiles in diamond and silicon using accelerating beams," *Appl. Phys. Lett.*, vol. 101, no. 7, pp. 71110, 2012.

[7] S. Jia, J. C. Vaughan and X. Zhuang, "Isotropic three-dimensional super-resolution imaging with a self-bending point spread function," *Nat. Photonics*, vol. 8, no. 4, pp. 302-306, Nov. 2014.

[8] G. A. Siviloglou, J. Broky, A. Dogariu and D. N. Christodoulides, "Observation of accelerating Airy beams," *Phys. Rev. Lett.*, vol. 99, no. 21, pp. 213901, Nov. 2007.

[9] E. Greenfield, M. Segev, W. Walasik and O. Raz, "Accelerating light beams along arbitrary convex trajectories," *Phys. Rev. Lett.*, vol. 106, no. 21, pp. 213902, May 2011.

[10] X. Chu, G. Zhou and R. Chen, "Analytical study of the self-healing property of Airy beams," *Phys. Rev. A*, vol. 85, no.1, pp. 013815, Jan. 2012.

[11] J. Broky, G. A. Siviloglou, A. Dogariu and D. N. Christodoulides, "Self-healing properties of optical Airy beams," *Opt. Express*, vol. 16, no. 17, pp. 12880-12891, Aug. 2008.

[12] M. Mazilu, D. J. Stevenson, F. Gunn-Moore and K. Dholakia, "Light beats the spread: "non-diffracting" beams," *Laser Photonics Rev.*, vol 4, no. 4, pp. 529-547, 2010.

[13] T. Melamed and A. Shlivinski, "Practical algorithm for custom-made caustic beams," *Opt. Lett.*, vol. 42, no. 13, pp. 2499-2502, July 2017.

[14] G. A. Siviloglou and D. N. Christodoulides, "Accelerating finite energy Airy beams," *Opt. Lett.*, vol. 32, no. 8, pp. 979-981, Apr. 2007.

[15] Y. Liang, Y. Hu, D. Song, C. Lou, X. Zhang, Z. Chen and J. Xu, "Image signal transmission with Airy beams," *Opt. Lett.*, vol. 40, no. 23, 5686-5689, Dec. 2015.

[16] G. Zhu, Y. Wen, X. Wu, Y. Chen, J. Liu and S. Yu, "Obstacle evasion in free-space optical communications utilizing Airy beams," *Opt. Lett.*, vol. 43, no. 6, pp. 1203-1206, Mar. 2018.

[17] G. A. Siviloglou, J. Broky, A. Dogariu and D. N. Christodoulides, "Ballistic dynamics of Airy beams," *Opt. Lett.*, vol. 33, no. 3, pp. 207-209, Feb. 2008.

[18] Y. Hu, P. Zhang, C. Lou, S. Huang, J. Xu and Z. Chen, "Optimal control of the ballistic motion of Airy beams," *Opt. Lett.*, vol. 35, no. 13, pp. 2260-2262, July, 2010.

[19] I. M. Besieris and A. M. Shaarawi, "A note on an accelerating finite energy Airy beam," Opt. Lett., vol. 32, no. 16, pp. 2447-2449, Aug. 2007.